

Resolving near-seabed velocity anomalies: Deep water offshore eastern India

Juergen Fruehn¹, Ian F. Jones¹, Victoria Valler¹, Pranaya Sangvai², Ajoy Biswal², and Mohit Mathur²

ABSTRACT

Imaging in deep-water environments poses a specific set of challenges, both in data preconditioning and velocity model building. These challenges include scattered, complex 3D multiples, aliased noise, and low-velocity shallow anomalies associated with channel fills and gas hydrates. We describe an approach to tackling such problems for data from deep water off the east coast of India, concentrating our attention on iterative velocity model building, and more specifically the resolution of near-surface and other velocity anomalies. In the region under investigation, the velocity field is complicated by narrow buried canyons (500 m wide) filled with low-velocity sediments, which give rise to severe pull-down effects; possible free-gas accumulation below an extensive gas-hydrate cap, causing dimming of the image below (perhaps as a result of absorption); and thin-channel bodies with low-velocity fill. Hybrid gridded tomography using a conjugate gradient solver (with 20-m vertical cell size) was applied to resolve small-scale velocity anomalies (with thicknesses of about 50 m). Manual picking of narrow-channel features was used to define bodies too small for the tomography to resolve. Prestack depth migration, using a velocity model built with a combination of these techniques, could resolve pull-down and other image distortion effects in the final image. The resulting velocity field shows high-resolution detail useful in identifying anomalous geobodies of potential exploration interest.

INTRODUCTION

Off the east coast of India, the transition from the shallower coastal waters to the deep shelf often involves significant topographical

variation in the seabed, which gives rise to numerous effects that must be dealt with by the processing geophysicist. In addition to deep channels and steep slopes, we encounter buried channels with low-velocity fills and gas hydrates. Diffracted and “out-of-plane” multiples are the norm in these environments (Stewart, 2004) and must be dealt with to derive a reliable velocity model so as to deliver an acceptable structural image (Stewart et al., 2007).

With the advent of 3D surface-related multiple elimination (SRME), a theoretically robust approach to complex multiple attenuation became available; and application of 3D SRME to these data proves to be very effective (Sangvai et al., 2008; Smith et al., 2008). The SRME technique, which the Delft University consortium pioneered (Verschuur et al., 1992), involves generating a model of the multiples from input data without prior knowledge of the velocity structure of the subsurface. Consequently, it is an ideal approach to accompany complex imaging problems when an a priori knowledge of the velocities cannot be assumed.

In the data considered here, the water depths range from a few hundred meters to more than 1 km; and for the most part they are deeper than 1.5 km, with deeply incised seabed channels running down the continental slope. The region under consideration is roughly 43 km by 54 km (some 2200 sq. km), covering a large exploration area of unknown hydrocarbon potential. Figure 1 shows a survey outline, indicating the locations of various inlines and crosslines that are discussed here. In addition, the lower left of the figure shows a canyon-fill geobody, which will be described later.

The data were collected in 2004 and imaged after 2D demultiple processing using 3D prestack time migration (PSTM). This time-domain imaging produced very good results overall, but it was considered suboptimal for specific parts of the region. The areas for which time migration constitutes an inadequate imaging solution are those areas affected by significant ray bending, such as directly below steep-sided seafloor canyons or beneath low-velocity geobody lenses. As with any complex or subtle imaging problem, the key to good imaging is the derivation of a representative velocity model. To ob-

Manuscript received by the Editor 23 November 2007; revised manuscript received 13 February 2008; published online 1 October 2008.

¹ION GX Technology, Egham, United Kingdom. E-mail: Juergen.Fruehn@iongeo.com; Ian.Jones@iongeo.com; Victoria.Valler@iongeo.com.

²Reliance Industries Ltd., Mumbai, India. E-mail: Pranaya.Sangvai@RIL.com; Ajoy.Biswal@RIL.com; Mohit.Mathur@RIL.com.

© 2008 Society of Exploration Geophysicists. All rights reserved.

tain such a model, we must produce clean, multiple-free prestack data. Thereafter, we can resort to prestack depth migration (PSDM) to image the subsurface, honoring the requisite ray bending.

Here, we demonstrate how velocity model building, using a combination of hybrid gridded tomography and detailed manual picking, can help resolve the various geophysical challenges encountered in this complex environment, leading to a satisfactory resolution of the imaging problem.

VELOCITY MODEL BUILDING AND PRESTACK DEPTH MIGRATION

In an environment with small-scale discontinuous velocity anomalies, such as those associated with narrow-channel fills or gas-hydrate accumulations, a purely layer-based velocity model would be inadequate (Jones, 2003; Fruehn et al., 2007). Furthermore, a purely gridded approach also might encounter problems (Jones et al., 2007). A layer-based approach assumes that all major velocity changes are bounded by geologic horizons. This can be appropriate for older consolidated sediments, as long as we do not have significant velocity variation within layers (other than a well-behaved, vertical compaction gradient).

A gridded model represents the subsurface velocity distribution with a cloud of values, decoupled from the sedimentary layers. It is of particular value in environments where the velocity field is dominated by the hydrostatic pressure gradient (typically in younger sediments), with velocities increasing more or less monotonically below the seabed. However, when we encounter significant lateral changes in compaction gradients (as in chalk layers in the North Sea), or have punctual intrusive bodies (such as salt in the Gulf of Mexico, or basalt), the purely layered and gridded approaches face limitations. The hybrid gridded approach (Jones, et al., 2007) attempts to combine both techniques by using a gridded tomographic solver but inserting layer constraints on the subsequent velocity update.

In this project, we used a hybrid gridded approach. We combined conventional gridded tomography, high-resolution gridded tomography, autopicked layers to serve as constraints within the tomography, and detailed manually interpreted layers to be inserted as the tops and bottoms of distinct regions in which a sufficiently resolved tomographic solution proved unobtainable. In this context, *high resolution* refers to solving the tomographic problem with 200-m cell dimension in x and y , and 20 m vertically, rather than the more usual 500-m lateral cell dimension with 100 m vertically.

The initial depth-interval velocity was derived from the PSTM time-stacking velocity (smoothed and converted to depth-interval velocity), and the water bottom was autopicked from a water-velocity depth migration and inserted in the initial model as an explicit layer. The water velocity was selected from a migration-perturbation scan (i.e., a suite of migrations using a percentage perturbation about some initial velocity function). As a result of this analysis, a constant value of 1500 m/s was selected. We noted that a velocity gradient in the water could be of use in imaging the seabed in neighboring areas, but here this was found to be unnecessary.

Following this, several iterations of gridded-tomographic model update were performed. This process involves running an autopicker (in this instance, based on plane-wave destructors: Claerbout, 1992; Hardy, 2003) on densely sampled Kirchhoff PSDM common-reflection-point (CRP) depth gathers, and inputting the autopicked velocity errors and dip information to the gridded-tomographic 3D solver. The solver uses a conjugate gradient (CG) technique to handle large volumes of 3D picks in the tomographic solution. For the model building and the final migration, an amplitude-preserving Kirchhoff implementation was used.

In Figure 2, we see a crossline from the 2004-vintage 3D Kirchhoff PSTM showing the complex seabed structure, along with evidence of the structural imprint of shallow-sediment velocity anomalies (dimming and pull-down indicated by the circles). The 2004 time-migration project used a dense, autopicked velocity field as part of the large-scale exploration project undertaken in the region by Reliance Industries.

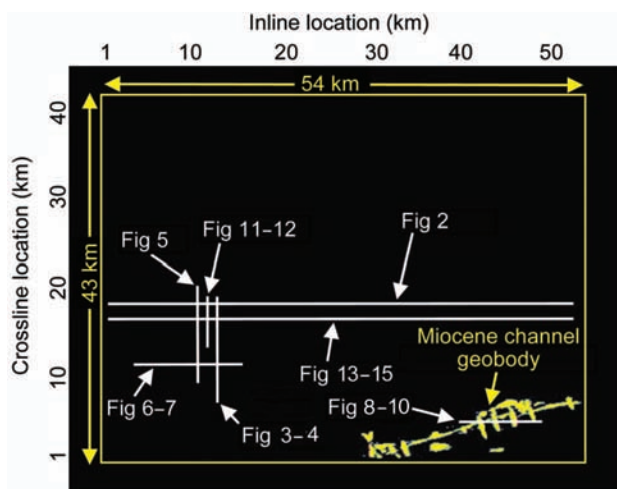


Figure 1. Survey map showing various inlines and crosslines described in this paper. Also seen in the lower right is the low-velocity geobody delineated by detailed picking on a grid on inlines and crosslines, outlining shallow canyon-fill sediments.

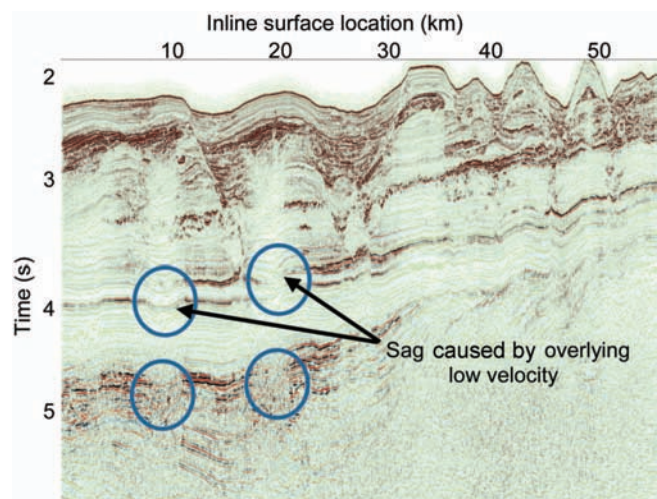


Figure 2. Three-dimensional crossline from the 2004-vintage 3D Kirchhoff PSTM (with 2D demultiple only), showing dimming and structural pull-down (sag) associated with shallower low-velocity anomalies (circled in the shallower part) and associated remnant multiple degradation of the deeper image below (also circled).

Figure 3 shows an inline from the vintage 3D PSTM. Many near-surface velocity anomalies are evident, some associated with possible gas-hydrate accumulations. The shallower (white) ellipse highlights a low-velocity geobody, which we infer has a possible component of free-gas accumulation associated with the gas-hydrate sealing layer as well as possible channel-fill water-saturated clay. Beneath this geobody, we have a region of dimming and can note velocity-related pull-down associated with this feature. The deeper ellipse highlights a zone degraded by remnant multiples.

Because of the degraded primary-signal content resulting from the overburden velocity anomaly, multiple energy dominates the contribution to the data in the deeper part of the section. Unless we could successfully attenuate the multiple, we would be unable to reveal the underlying geologic structure. Aliasing of the multiple moveout behavior in deep water results in a stack response, showing a broken reflector character. For successful model building, such noise first must be removed in the prestack domain; and in the PSDM project described here, 3D SRME was used successfully to achieve this.

In Figure 4, we see the same inline as in Figure 3, after final 3D PSDM imaging with all preprocessing (including 3D SRME). The pull-down has been resolved and deeper imaging improved (indicated in the ellipse at about 4-km depth). To achieve this imaging improvement, the velocity model building required several phases, using different techniques.

First, three iterations of purely gridded high-resolution CG tomography were used to refine the sediment velocity field below the autopicked (highly structured) seabed. These iterations used picks with a 200×200 -m lateral and 20-m vertical spacing. Following this, CG tomography (on a $500 \times 500 \times 100$ -m grid) was used to determine the velocity structure in the larger and deeper low-velocity geobodies (lying mostly a kilometer or more below the seabed). In some areas, a series of Mio-Pliocene channels were visible; and

these were resolved by detailed manual picking in conjunction with a migration velocity-perturbation scan.

Gas hydrates

Clathrates, such as methane hydrates, often form in deep-water regions with unconsolidated sediments when the temperature and pressure are appropriate (Carcione and Tinivella, 2000; Chopra et al., 2003). In this area of offshore India, they can occur below a water depth of about 600 m (Chaudhuri et al., 2002). The clathrate itself forms an impermeable high-velocity (usually thin) layer, and below this, we sometimes see an accumulation of free gas, giving rise to a low-velocity zone immediately below the high-velocity clathrate layer.

A seismic characteristic of these accumulations is that they can crosscut the sedimentary layering (so they can look like a multiple or remnant bubble-energy in that regard), and occur about 150–250 meters below the seabed (as indicated in Figure 5). As a reflection event, they subparallel the seabed. They are referred to as a *bottom-simulating reflector* (BSR). The BSR forms when temperature and pressure conditions are such that clathrates form. These frozen, typically methane-hydrate structures can crosscut the geologic strata; and given that they are primarily controlled by the hydrostatic pressure gradient below the seabed, they tend to be subparallel to the seabed contours. Hence we see a reflector tracking the seabed structure, crosscutting the sedimentary depositional layers.

For velocity anomalies related to the gas hydrate, we relied primarily on high-resolution gridded tomography. We could resolve small-scale velocity features (scale length of <1 km) with interval velocity about 1250 m/s in the underlying free-gas zones, compared with the background-sediment velocities of about 1600 m/s. These possible free-gas accumulations (or water-saturated clays) have an associated pull-down in the time section, as well as amplitude dimming and loss of high frequencies.

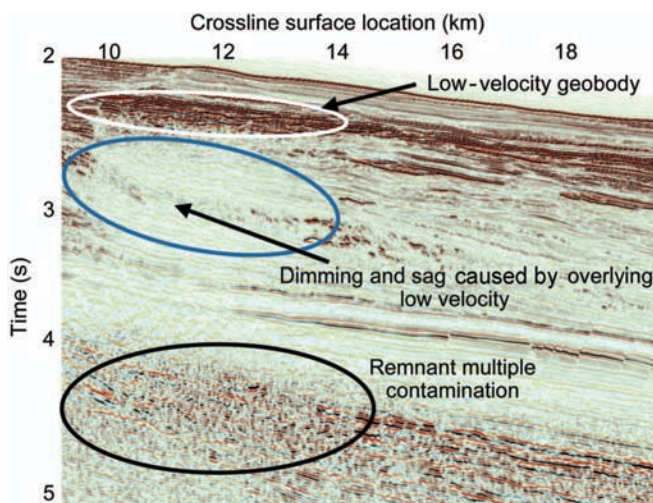


Figure 3. Vintage 2004 3D PSTM inline (with 2D demultiple only). Dimming below a shallow geobody is evident (circled); and below, remnant multiple contamination degrades the image (circled).

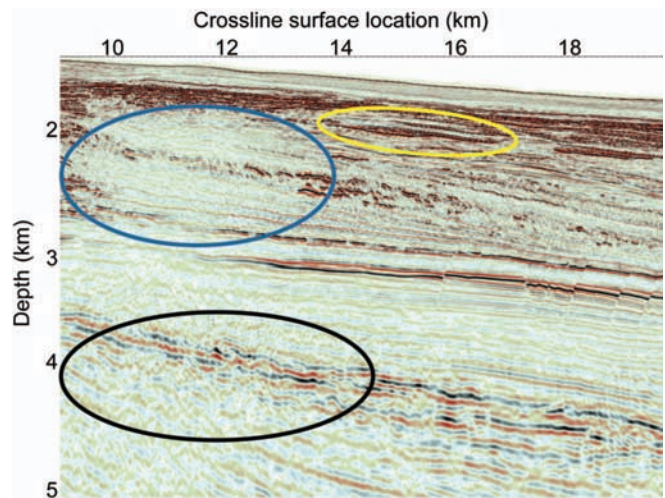


Figure 4. New 3D PSDM from same inline as Figure 3, following 3D SRME. The slight sag is mostly resolved, and remnant multiple contamination is mostly removed by the 3D demultiple, allowing a reasonable image to be obtained. The feature encircled in the rightmost shallow yellow ellipse is described in more detail in Figures 11 and 12.

Figure 5 details the analysis of a probable gas-hydrate accumulation and associated free-gas zone. In the time-migration image (left), we can discern an event parallel to the seabed about 200 m below the seafloor (denoted by the dotted orange line). This event is probably a

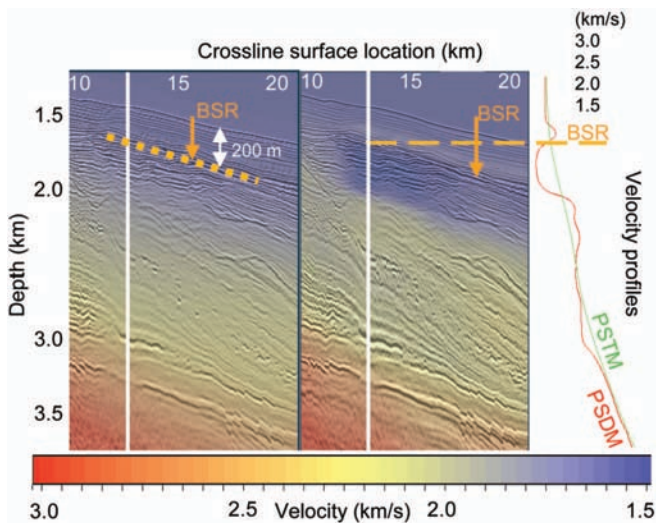


Figure 5. The smooth velocity field derived for time-domain migration (leftmost PSTM seismic section) does not require high-resolution detail. For depth imaging, the velocity-estimation techniques used are capable of providing the higher-resolution detail required for more demanding depth imaging (central PSDM seismic section). On the right, we see the smooth velocity profile from the PSTM (in green) and the more detailed velocity profile from the tomographic PSDM model building (in red). This could be interpreted as a characteristic high-velocity clathrate cap and an underlying low-velocity free-gas zone (these observations and inferences are speculative). The solid white vertical lines on the seismic sections indicate the locations in which these velocity profiles are extracted.

BSR, a characteristic of gas-hydrate formation. In the corresponding image from the depth migration (center panel), the resolution of the detailed velocity structure helps to clarify the deeper part of the image and to resolve associated pull-down.

The vertical white line indicates where we extracted the velocity profiles associated with the PSTM and PSDM velocity models. These profiles are plotted on the right of the figure. The PSTM profile is smooth and featureless, but the PSDM profile shows a high velocity kick at about 1600-m depth (~250 m below the seabed), immediately followed by a low-velocity zone of about 300-m vertical extent. These features are characteristic of free-gas accumulation below a high-velocity gas-hydrate cap, and they have been encountered elsewhere in this region. When overpressured, such gas accumulations can constitute a severe geohazard.

In Figure 6, we see the initial model (picked seabed and smooth velocity field from the vintage PSTM) superimposed on the associated 3D PSDM result. The shallow-sediment package, encircled, causes a pull-down in the underlying sediments (highlighted by the deeper ellipse). By the second iteration of tomography, we begin to resolve this pull-down as the tomography yields a low-velocity geobody, with a minimum interval velocity of ~1300 m/s compared to the surrounding sediment velocity of 1600 m/s (Figure 7).

Channel fills

For intricate narrow channels present in the Mio-Pliocene section just below the seabed, we relied on manual interpretation of the top and base of the channel features to define their geometry, combined with a scan over potential channel-fill velocities. Because of the small scale of these features, a purely gridded-tomographic approach was unable to resolve the required detail. The channels were picked on a dense localized grid of inlines and crosslines.

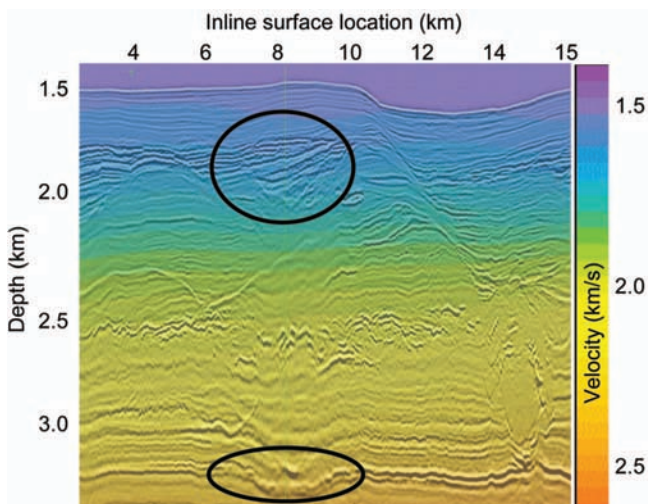


Figure 6. Three-dimensional PSDM using initial model, showing evidence of pull-down (highlighted in the lower ellipse) resulting from a shallow velocity anomaly (highlighted in the shallower ellipse).

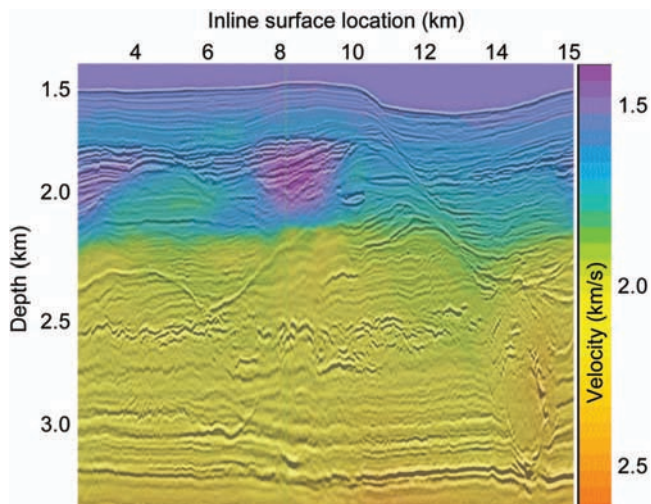


Figure 7. Three-dimensional PSDM after second iteration attempting to resolve pull-down. The pull-down near 3-km depth has been mostly corrected, as the velocity in the shallow geobody has been reduced from about 1600 m/s to ~1400 m/s.

Figure 8 shows the first kilometer of data near the seabed, where we see deeply incised seabed canyons, but also some small localized channels just below the seabed. These channels result in a severe pull-down distortion of the underlying sediments resulting from their low-velocity fill. If we were to use a smooth velocity model, we would be unable to resolve these small-scale features (typically 300 m–400 m in width); hence detailed manual picking is required. The 3D PSDM image shown in Figure 8 was created using a smooth-background velocity field (hence the pull-down is visible). The detailed channel-fill velocity model is superimposed (not the velocity used for this migrated image). A migration velocity scan was used to determine the best channel-fill interval velocity; in this case, 1200 m/s was used.

Figures 9 and 10 compare the 3D PSDM results after migrating with a smooth-background velocity field (no punctual channels included) versus the result incorporating the low-velocity fill channels. The improvement in the deeper section, below about 2-km depth, is significant. We have not perfectly resolved the shallow-channel problems, but incorporating them in this way enables better resolution in the deeper section. Ignoring them is not a viable option.

Underlying low-velocity canyon fills

Below the younger Pleistocene section, we have channel-like features. These might be sand bearing and possibly gas charged; they could be potential exploration targets, or alternatively, they could be water-saturated clay bodies (see, for example, the geobody highlighted in the yellow ellipse in the upper right of Figure 4). These were also the focus of some attention, and high-resolution tomography was used to define some of these features.

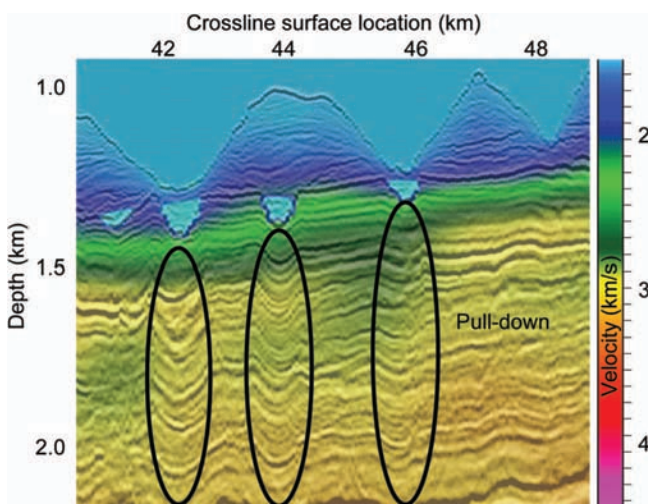


Figure 8. Picked canyon-fill events (four pale-blue features just below the seabed) with color overlay of the final selected velocity-fill model, superimposed on an initial PSDM crossline produced by using a smooth velocity model (hence clearly showing the pull-down problems).

In Figure 11, we see CRP gathers and the associated PSDM image with velocity overlay. The velocity here is from a purely gridded CG tomography on a $500 \times 500 \times 100$ -m input-pick cell size. A thin sand lens (50 m thickness) can be seen in the lower image, but it has not been resolved in the current iteration. The gathers shown in the upper portion of the figure are undercorrected at the top of the lens feature (velocity at this depth is too low), and the gathers for the base of the event are flat.

Conceptually, we can imagine that increasing the velocity above the feature (so as to flatten the gathers for the top of the channel)

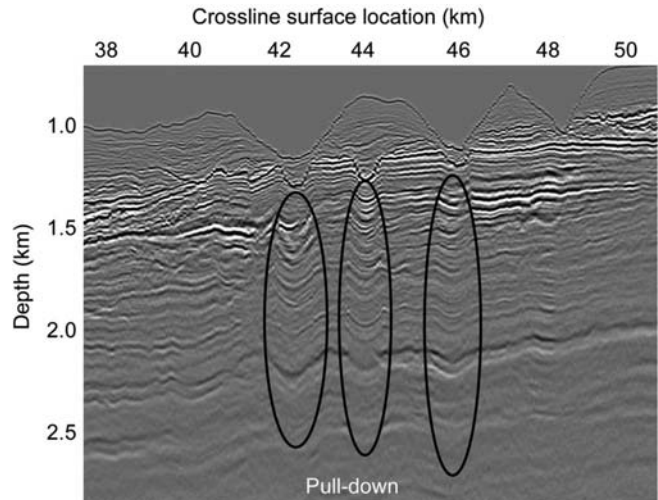


Figure 9. Three-dimensional PSDM crossline with smooth-background model. Numerous probable pull-down features can be identified. Imaging below these features is problematic.

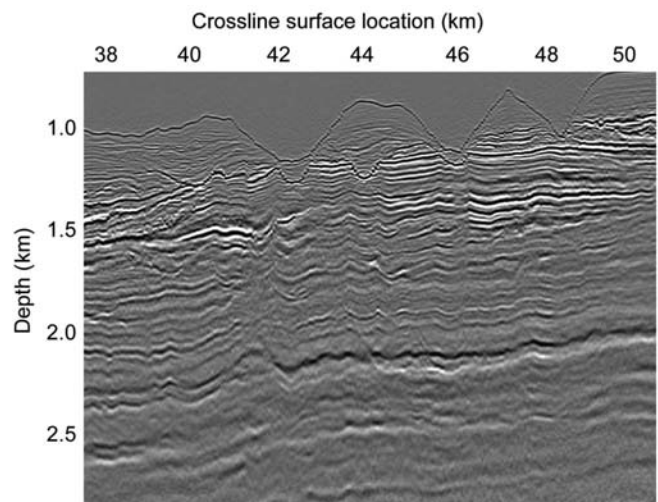


Figure 10. Three-dimensional PSDM crossline with detailed low-velocity channel-fill model. Sags are greatly reduced, and deeper imaging is clearly improved.

would cause the base-channel gathers to curl down (too fast); so we also need to reduce the channel-fill velocity while increasing the velocity above the channel. This was accomplished in the next iteration (as shown in Figure 12), where the lateral dimensions of the tomographic

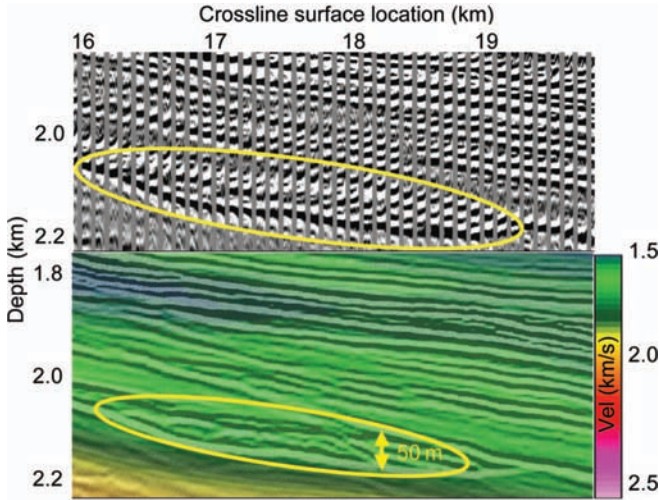


Figure 11. Top: CRP gathers after the fourth run of PSDM (these gathers are used as input to the next iteration of tomographic-model update). We can see some residual velocity error (gathers curling upward indicates the velocity is still too low) above the channel. Bottom: Image associated with these gathers with interval-velocity color overlay. The thin-lens feature (encircled) is seen in a larger context in the upper right of Figure 4.

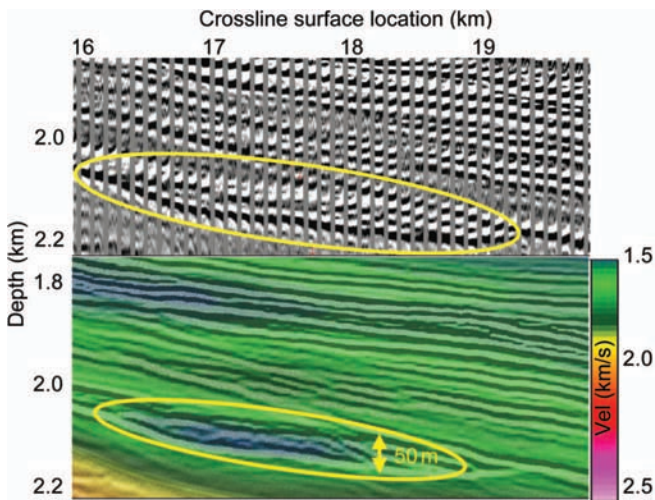


Figure 12. Top: CRP gathers after the subsequent update of 3D CG tomography. Some of the undercorrection above the channel has been resolved and the channel velocity itself lowered, so as to preserve flat gathers at the channel base. Bottom: Image associated with these gathers with interval-velocity color overlay, showing the low velocity in the thin-channel feature. The thin feature (encircled) is seen in a larger context in the upper right of Figure 4.

cell were reduced to 200 m and the vertical dimension to 20 m. We consider this to be close to the vertical resolution of our technique.

Model evolution

In the following figures, showing a long crossline adjacent to that of Figure 2, we summarize the evolution of the model. Figure 13 (top and bottom) compares the first and second iterations, which dealt with only the shallow section, while Figures 14 and 15 compare the overall section. By the fifth iteration, the deep section has been improved considerably. During the model building of the shallow section, the data preprocessing was ongoing so as to apply lengthy processes such as 3D SRME and the other denoise steps. These fully preprocessed data then were used for deeper model update and the final imaging.

As a consequence, the data input to the earlier model-building iterations did not have the full denoise preprocessing sequence applied. This is reasonable for deep-water environments, as we have much work to do in model building before encountering the first multiple. Overlapping the preprocessing and model building in this way also facilitates reduction of overall turnaround time.

It is important to note that, for a global tomographic solution, all parts of the model can be adjusted at each iteration. Hence we can see subtle changes in the shallow section for some parts of the model, even at the latter iterations. Once we have imposed a layer constraint in the hybrid scheme (such as for the seabed or detailed picked channels), those parts of the model remain invariant. The update scheme ceases to be a truly global one and thus can be viewed as a class of layer stripping (although we have much more flexibility in a gridded scheme than in a purely layer-based scheme).

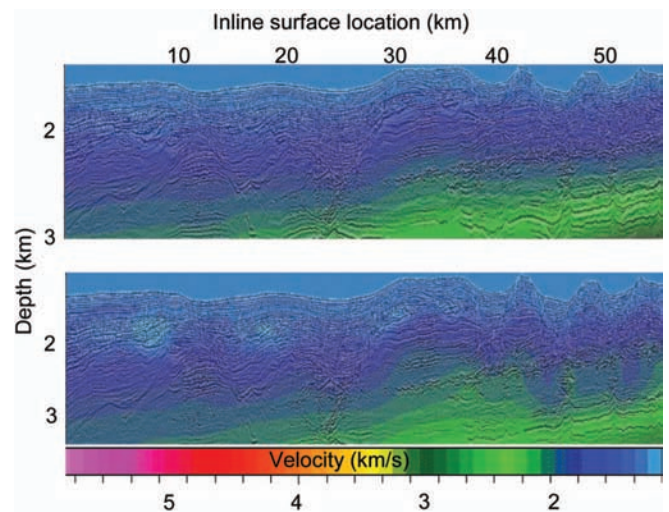


Figure 13. Upper panel: First iteration of model update for PSDM crossline down to 3 km. Lower panel: Second iteration of model update down to 3 km. For the most part, the structural imprint of the seabed and underlying sediments has been removed. Both images shown with interval-velocity color overlay.

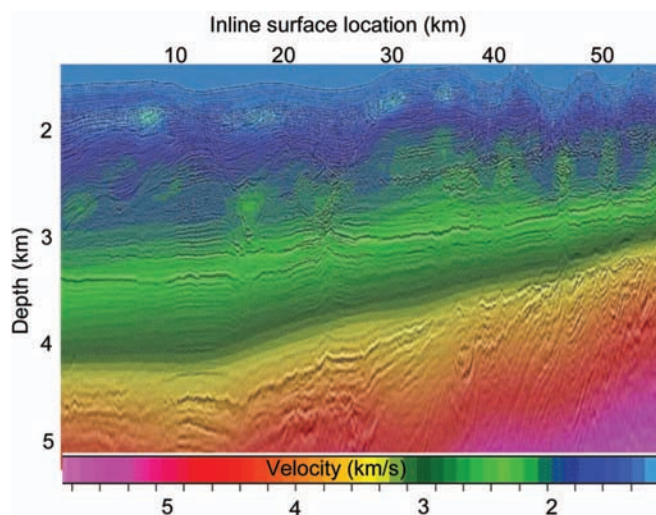


Figure 14. The whole crossline section for iteration 4, with interval-velocity color overlay.

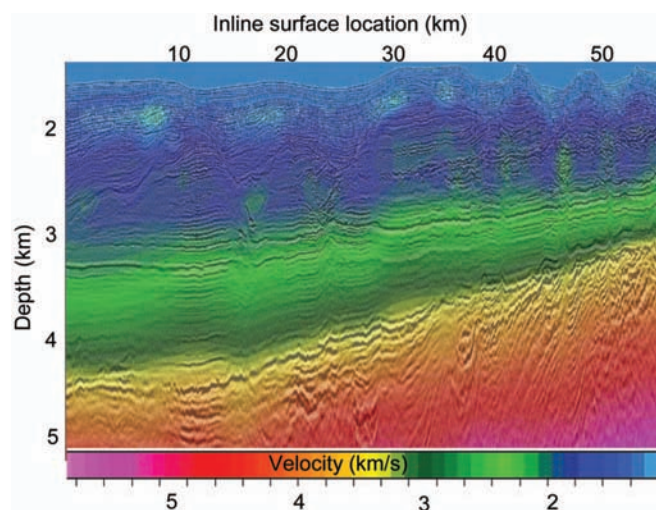


Figure 15. The whole crossline section for iteration 5, with interval-velocity color overlay. The majority of the structural imprint of the overburden has been removed.

CONCLUSIONS

For imaging in complex environments, it is necessary to use a wide range of tools for suppression of the various classes of noise and multiples. This must be accomplished in the prestack domain so that automated dense picking can be performed on migrated gathers to permit reliable model update. In deep-water areas, we are fortunate that the water-bottom multiple problem does not affect much of the data, so we can proceed with model building for the data above the time of the first water-bottom multiple while demultiple processing is proceeding in parallel. However, we still need to address internal multiple and other noise problems.

In addition, a flexible approach to model update is required, permitting us to incorporate small-scale punctual velocity features, such as those associated with low-velocity channel fills, as well as resolving the gradual lateral and vertical changes associated with broader structural trends. At some short-scale lengths, a tomographic solution is unlikely to be capable of resolving important velocity detail, and in these instances it is important to be able to incorporate velocity information from other sources. In this case study, we have embedded into the model a network of narrow channels, defined by detailed picking of their tops and bases from a dense grid of inlines and crosslines.

Utilization of such an approach for data offshore of eastern India has resulted in an improvement in image quality compared to a recent prestack time migration, avoiding the structural distortion introduced by localized velocity variation in the near-surface sediments.

ACKNOWLEDGMENTS

We express our thanks to colleagues at Reliance Industries and ION GX Technology for help and advice during this project. We thank especially Phil Smith at GXT, who ran the preprocessing, and our respective employers for permission to present this work. We thank also the SEG reviewers, Andreas Ruger and Sylvestre Charles, and the associate editors, Tamas Nemeth and Bill Harlan, for their insightful comments and encouragement.

REFERENCES

- Carcione, J. M., and U. Tinivella, 2000, Bottom-simulating reflectors: Seismic velocities and AVO effects: *Geophysics*, **65**, 54–67.
- Chaudhuri, D., N. Lohani, S. Chandra, and A. Sathe, 2002, AVO attributes of a bottom simulating reflector: East coast of India: 72nd Annual International Meeting, SEG, Expanded Abstracts, 300–303.
- Chopra, S., V. Alexeev, and Y. Xu, 2003, Successful AVO and cross-plotting: *Recorder*, **28**, no. 9, 5–11.
- Claerbout, J. F., 1992, *Earth soundings analysis: Processing versus inversion*: Blackwell Scientific Publications.
- Fruehn, J., H. Sherazi-Selby, P. Hardy, J. Tryti, and N. Steinsland, 2007, High-resolution velocity model building for pre-stack depth migration in the Nordsjon area, Norwegian North Sea: 69th EAGE Conference and Exhibition, Extended Abstracts, paper C043.
- Hardy, P. B., 2003, High resolution tomographic MVA with automation: SEG/EAGE Summer Research Workshop, Trieste, Extended Abstracts, paper T27.
- Jones, I. F., 2003, A review of 3D preSDM velocity model building techniques: *First Break*, **21**, no. 3, 45–58.
- Jones, I. F., M. J. Sugrue, and P. B. Hardy, 2007, Hybrid gridded tomography: *First Break*, **25**, no. 4, 15–21.
- Sangvai, P., A. Biswal, M. Mathur, J. K. Fruehn, P. Smith, D. G. King, I. F. Jones, and M. C. Goodwin, 2008, Complex imaging challenges: Offshore South East India: Proceedings of the 7th biennial meeting of the Society of Petroleum Geophysicists, paper P38.
- Smith, P., I. F. Jones, D. G. King, P. Sangvai, A. Biswal, and M. Mathur, 2008, Deep water pre-processing, East Coast India: *First Break*, **26**, no. 5, 101–107.
- Stewart, P., 2004, Multiple attenuation techniques suitable for varying water depths: Proceedings of the Canadian Society of Exploration Geophysicists annual meeting.
- Stewart, P. G., I. F. Jones, and P. B. Hardy, 2007, Solutions for deep water imaging: *Geohorizons*, **12**, no. 1, 8–22.
- Verschuur, D. J., A. J. Berkhout, and C. P. A. Wapenaar, 1992, Adaptive surface-related multiple elimination: *Geophysics*, **57**, 1166–1177.